

# **SERDP SEED Project UX-1284: APPLICATION OF WAVELETS FOR DETECTION AND DISCRIMINATION OF UXO**

B. Damiano and R. W. Tucker, Jr., Engineering Science and Technology Division  
W. E. Doll and A. M. Emond, Environmental Sciences Division

Oak Ridge National Laboratory, Oak Ridge, Tennessee 37831-6010  
August 2003

## **1 - INTRODUCTION**

This report summarizes the results of the SERDP SEED Project UX-1284, Application of Wavelets for Detection and Discrimination of UXO. This project addressed the Statement of Need (SON) for SERDP's SEEDSON-02-04, which calls for improved signal processing and or sensors to aid in discrimination of clutter from ordnance in contaminated areas where overlapping signatures are common. We investigated the effectiveness of signal processing techniques based on wavelets (1) to improve the signal to noise ratio and extract additional information from the signals and (2) as part of a probability-based approach for discriminating between ordnance and clutter.

Previous work with wavelet-based signal processing has shown the ability of wavelet-based filtering techniques to significantly increase the signal to noise ratio, allowing weak, but real, signals to be extracted from noisy backgrounds. The increase in the signal to noise ratio is also expected to result in a more accurate and detailed description of magnetic anomalies that are currently detectable. This increase in available detail may make it easier to distinguish between multiple overlapping anomalies.

Improved methods for detection and discrimination of UXO are desirable because the size of the ordnance contaminated areas are large - estimated by the U.S. DoD to be approximately 11 million acres (roughly equal to the combined areas of the states of Vermont and New Hampshire). If successful, this demonstration will make the accuracy of reconnaissance of unexploded ordnance using airborne methods more comparable to ground-based detection methods, and provide a method for improving the detection and discrimination capabilities of ground-based methods.

This report is organized as follows: Section 2 presents background information on wavelets, wavelet decomposition using dyadic wavelets and wavelet packets, and describes the application of probabilistic methods for classification. Section 3 describes the project activities associated with applying wavelet filtering to airborne magnetic data. The selection of the wavelet-filtering scheme is described and results from wavelet filtering are presented and compared to standard filtering results. Section 4 describes the project activities associated with discrimination of ordnance from clutter using probabilistic methods. The main focus of this effort was limited to wavelet-based descriptor selection. Section 5 presents conclusions and recommendations based on the project results.

## 2 - BACKGROUND INFORMATION

### 2.1 Wavelet Transform Description

In wavelet decomposition, the signal is expanded in a set of orthonormal, compactly supported basis functions. This property allows wavelets to preserve both time (spatial) and frequency information. The ability to preserve time information makes the wavelet transform particularly useful for describing transient or non-stationary data and for describing data sets containing discontinuities.

The orthonormal basis used in the wavelet decomposition is based on a single function  $\psi(t)$  that is defined recursively by dilation and scaling

$$\psi_{a,b}(t) = \frac{1}{\sqrt{a}} \psi\left(\frac{t-b}{a}\right), \quad (1)$$

where  $a$  specifies the wavelet scale and  $b$  specifies the wavelet translation.<sup>1</sup> The continuous wavelet transform of a signal  $x(t)$  is defined as

$$x_{\psi}(a,b) = \int_{-\infty}^{\infty} \psi_{a,b}^*(t) x(t) dt. \quad (2)$$

The continuous wavelet transform can be extended to a discretely sampled data set  $x(t)$  of  $N$  samples defined as

$$x(t) = x_n = x(t_n), \quad t_n = n\Delta t, \quad n = 1, 2, \dots, N, \quad (3)$$

where  $\Delta t$  is the sampling interval. It can be shown that if the scale  $a$  and the shift  $b$  are discretized by using

$$a = 2^j \Delta t, \quad b = \frac{k}{2^j} \Delta t, \quad (4)$$

where  $j$  and  $k$  are integers, an orthonormal basis function  $\psi_{jk}$  can be derived;

$$\psi_{j,k} = \frac{2^{\frac{j}{2}}}{\sqrt{\Delta t}} \psi(2^j n - k). \quad (5)$$

The discrete wavelet transform is then given by the summation

$$d_{j,k} = \sqrt{\Delta t} \sum_{n=0}^{N-1} 2^{\frac{j}{2}} \psi^*(2^j n - k) x_n, \quad (6)$$

where the wavelet transform coefficients are denoted by  $d_{j,k}$ . The wavelet function is defined by a set of quadrature mirror filter coefficients. Furthermore, Daubechies has

shown that these filter coefficients can be selected such that the resulting wavelet has  $M$  vanishing moments, that is

$$\int_{-\infty}^{\infty} \psi(x) x^m dx = 0, m = 0, 1, \dots, M - 1. \quad (7)$$

Wavelet functions with compact support and vanishing moments result in local events affecting only a limited number of wavelet coefficients and in smooth portions of the signal being accurately represented by few coefficients. These properties are useful for data compression and for denoising signals because virtually all the significant information is contained in relatively few wavelet coefficients. The remaining coefficients contain noise and can be set equal to zero, effectively eliminating the noise.

The application of the wavelet decomposition (or wavelet filter) results in two subbands, each with half the bandwidth of the original signal. The high-frequency subband is generally referred to as "signal details"; if the highest frequency contained in the original signal is  $\omega_{hi}$ , the frequency range in this subband extends from  $\omega_{hi}/2$  to  $\omega_{hi}$ . The low-

frequency subband is referred to as the "signal approximation" and has a frequency range of 0 to  $\omega_{hi}/2$ . Each subband has half the number of samples as the original signal.

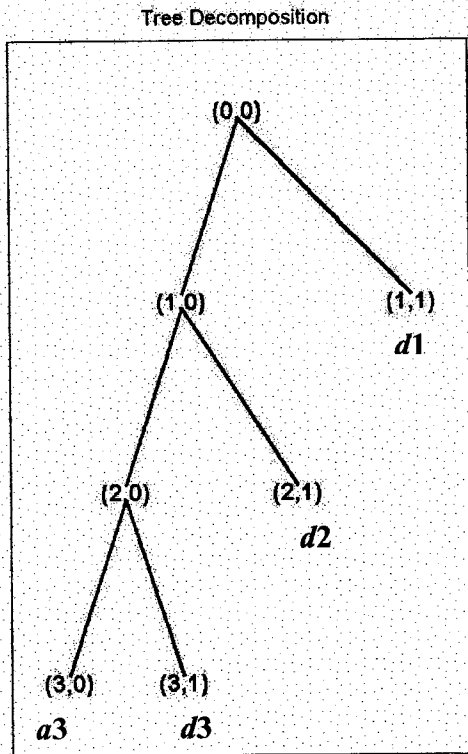


**Figure 1. Three-level dyadic tree.**

detail subband,  $d1$ , contains  $N/2$  elements, the second level detail subband,  $d2$ , contains  $N/4$  elements, and the third level detail subband,  $d3$ , and third level approximation subband,  $a3$ , each contain  $N/8$  elements. If the original signal has time increment of  $\Delta t$  between samples,  $d1$  has a

In the dyadic wavelet transform, the wavelet decomposition is recursively applied to the signal approximation a specified number of times. Each application of the wavelet decomposition results in formation of a wavelet level, with each level composed of a detail subband and an approximation subband. The approximation subband is then operated on again by the wavelet decomposition, forming the next wavelet level.

Figure 1 shows a 3-level dyadic wavelet transform tree. If the original signal has  $N$  samples, the first level detail subband, identified as  $d1$ , contains  $N/2$  elements, the second level detail subband,  $d2$ , contains  $N/4$  elements, and the third level

time increment of  $2\Delta t$  between samples,  $d2$  has a time increment of  $4\Delta t$  between samples, and  $d3$  and  $a3$  have a time increment of  $8\Delta t$  between samples. In an  $m$ -element dyadic wavelet transform, the wavelet decomposition is applied  $m$  times and each detail subband contains half as many elements as the previous detail subband. Table 1 shows the number of elements, the frequency range, and the time between elements for each of the subbands in the 3-level dyadic wavelet transform.

## 2.2 Wavelet Packet Description

subband	number of elements	frequency range	time increment between elements
original signal	$N$	$0 - \omega_{hi}$	$\Delta t$
$d1$	$N/2$	$\omega_{hi}/2 - \omega_{hi}$	$2\Delta t$
$d2$	$N/4$	$\omega_{hi}/4 - \omega_{hi}/2$	$4\Delta t$
$d3$	$N/8$	$\omega_{hi}/8 - \omega_{hi}/4$	$8\Delta t$
$a3$	$N/8$	$0 - \omega_{hi}/8$	$8\Delta t$

**Table 1. Number of elements, frequency range, and time increment for the subbands of the 3-element dyadic wavelet transform.**

The wavelet packet is much like the dyadic wavelet transform, except the wavelet decomposition is applied to the detail subbands as well as to the approximation subbands. Figure 2 shows a 3-level wavelet packet tree. The result of the wavelet packet decomposition is the subbands  $a3$ ,  $d31$ ,  $d32$ ,  $d33$ ,  $d34$ ,  $d35$ ,  $d36$ , and  $d37$ . In an  $m$ -element wavelet packet transform, the wavelet decomposition is applied  $2^m$  times and all subbands contain the same number of elements, have the same time increment between elements, and have equal bandwidths. Table 2 shows the number of elements, the frequency range, and the time increment between elements for each wavelet packet subband.

Comparison of the dyadic wavelet transform and the wavelet packet transform shows that the wavelet packet transform requires considerably more computations and results in a finer frequency decomposition and a coarser time decomposition.

The choice of using either the dyadic wavelet transform or the wavelet packet transform will obviously be problem-dependent. Wavelet filtering of magnetometer data requires a relatively fine frequency decomposition in order to remove helicopter rotor noise without seriously affecting the frequency range containing UXO anomaly information. For this reason, we have selected the wavelet packet transform for wavelet filtering.

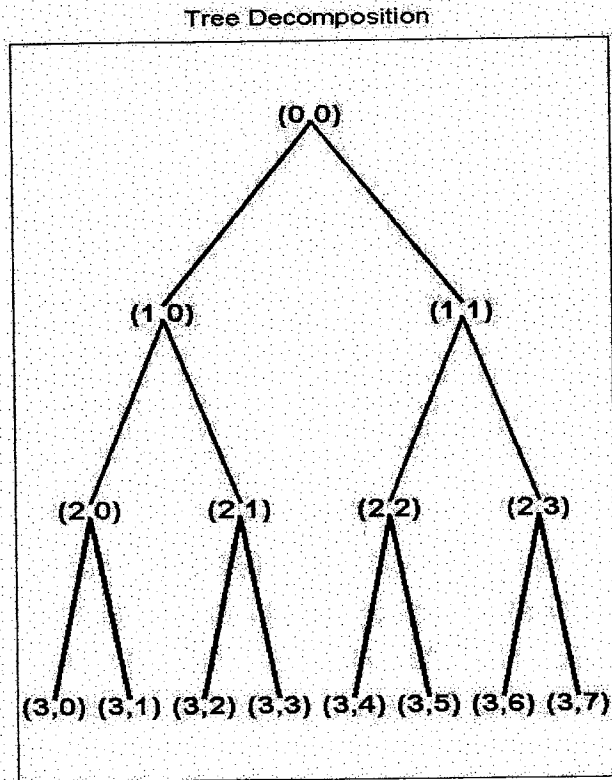


Figure 2. Three level wavelet packet tree.

subband	number of elements	frequency range	time increment between elements
original signal	$N$	$0 - \omega_{hi}$	$\Delta t$
$d31$	$N/8$	$\omega_{hi}/8 - \omega_{hi}/4$	$8\Delta t$
$d32$	$N/8$	$\omega_{hi}/4 - 3\omega_{hi}/8$	$8\Delta t$
$d33$	$N/8$	$3\omega_{hi}/8 - \omega_{hi}/2$	$8\Delta t$
$d34$	$N/8$	$\omega_{hi}/2 - 5\omega_{hi}/8$	$8\Delta t$
$d35$	$N/8$	$5\omega_{hi}/8 - 3\omega_{hi}/4$	$8\Delta t$
$d36$	$N/8$	$3\omega_{hi}/4 - 7\omega_{hi}/8$	$8\Delta t$
$d37$	$N/8$	$7\omega_{hi}/8 - \omega_{hi}$	$8\Delta t$
$a1$	$N/8$	$0 - \omega_{hi}/8$	$8\Delta t$

Table 2. Number of elements, frequency range, and time increment for the subbands of the three-element wavelet packet transform.

## **2.3 Application of Probabilistic Methods for Classification**

Applying probabilistic methods for classification involves several steps. First, a set of descriptors that adequately distinguish between classes must be identified. Next, the statistical properties of the descriptor set for each class must be determined, usually by measuring the descriptors for samples taken from members of each class and calculating the usual statistical quantities such as the average and standard deviation. Finally, a statistical test is developed using the descriptor statistical properties to determine class membership of an unknown sample.

Our original intention in this project was to perform all three steps for a limited number of samples of both ordnance and clutter. Unfortunately, because of unexpected difficulty in the performance of the wavelet filtering portion of the project, we were forced to focus only on the identification of the descriptor set. It has been our experience that if an adequate descriptor set can be identified, that is, one that can distinguish between the classes, then the other two steps involved in applying probabilistic classification methods will present little difficulty. By focusing our effort on the key step in the process, we feel we can most effectively evaluate the potential for applying probabilistic methods for classification of ordnance and clutter, given the project constraints.

## **3 - WAVELET FILTERING OF AIRBORNE MAGNETOMETER DATA**

### **3.1 Approach**

The wavelet filtering should retain signal features containing magnetic anomaly information while removing noise and signal features describing other phenomena such as rotor noise, large-scale magnetic effects, etc. The approach used to determine the optimum wavelet-filtering scheme was as follows:

- 1) Generate synthetic data for several magnetic anomalies using the MAGMOD computer code. Three different ordnance types buried at three different depths were used, resulting in 9 synthetic magnetic anomalies.
- 2) Extract a pure noise signal from the measured magnetometer data. A portion of the magnetometer signal collected at an altitude greater than 10 meters was used as the noise signal. Experience shows that magnetic anomalies indicative of UXO are not detectable at altitudes greater than 10 meters, thus the magnetometer measurements at altitudes greater than 10 meters contains only effects such as rotor noise and large-scale magnetic anomalies.
- 3) Apply the wavelet packet decomposition to each signal and calculate the energy contained in each subband. Ideally, we would find no overlap in subband signal energy between the two signals.

4) The optimum wavelet-filtering scheme would retain the subbands containing high synthetic signal energy and discard subbands containing high noise signal energy. The filtered signal is formed by inverse wavelet transforming the retained subbands.

5) The effectiveness of the wavelet-filtering scheme can be evaluated by comparing the wavelet filtering results to standard filtering results. Although wavelet filtering will be performed using profile data, the comparison can also be performed after converting the signals to gridded data. The wavelet filtering would be considered superior to standard filtering if

- a) additional anomaly detail can be discerned in the wavelet filtered results,
- b) additional anomalies can be detected in the wavelet filtered results,
- c) the overall noise level is reduced in the wavelet filtered results, or
- d) the application of wavelet filtering is significantly faster or requires significantly less user intervention during the filtering process.

The wavelet analysis is described in the next section. Descriptions of the synthetic and noise signals are given and the results of the wavelet packet analysis for each signal are presented. The selection of the wavelet-filtering scheme is described and the results of this scheme applied to the synthetic signal with added noise are shown. Section 3 describes the magnetometer data used in to compare the filtering and shows the results of the wavelet-filtering scheme on the collected data. A comparison of the wavelet-filtered and standard-filtered data is given for both profile and gridded data. Conclusions and a summary of the analysis results are contained in the final section.

### **3.2 Wavelet Filtering Scheme Selection**

The wavelet-filtering scheme was selected after examining the energy in the wavelet subbands for the synthetic signal, which contains only anomaly signatures, and a pure noise signal. For each signal, a four level wavelet packet decomposition was performed on the synthetic data using a Daubechies-20 coefficient wavelet.

#### **3.2.1 Synthetic Signal**

The MAGMOD computer code was used to calculate the magnetometer responses of for three different ordnance types buried at three different depths. The synthetic signal is shown in Figure 3.

The sample number corresponds to the sensor traveling from south to north; that is, the first data point represents the southernmost point. There are 9 different magnetic anomalies from bodies centered every 50 m from  $x = 0$ , i.e. at  $x = (0,50,100,...400)$ . The sample number corresponds to the sensor traveling from south to north; that is, the first data point represents the southernmost point. There are 9 different magnetic anomalies from bodies centered every 50 m from  $x = 0$ , i.e. at  $x = (0,50,100,...400)$ . The three southernmost anomalies are from 76-mm ordnance 1.5, 2.5, and 3.5 m from the

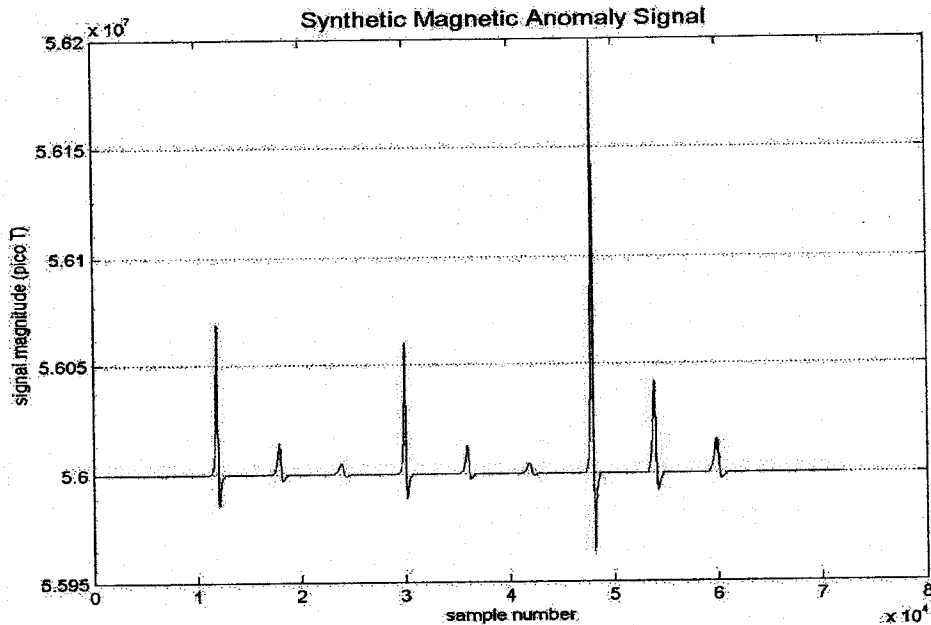


**Figure 3. The MAGMOD-calculated synthetic magnetic anomaly signal.**

sensor. The next three anomalies are from 105-mm ordnance 1.5, 2.5, and 3.5 m from the sensor. The three northernmost anomalies are from 155-mm ordnance 1.5, 2.5, and 3.5 m from the sensor. These depths correspond to a flight height of 1.5 m above ground level and burial depths of 0, 1, and 2 m. Each object is angled 45 degrees below horizontal, pointed north-south with the southernmost end of the ordnance nearest the surface. The ambient magnetic field is 56000 nT, has a declination of 0 degrees, and an inclination of 70 degrees. The helicopter velocity was assumed to be 10 m/sec and the sample rate was 60 Hz.

The four-level wavelet packet tree representing the wavelet decomposition of the signal is shown in Figure 4. Each branch point represents a time series obtained from wavelet decomposition. For example, the original time series, represented by (0,0), is decomposed into two subbands, (1,0) and (1,1). The (1,0) time series is then decomposed into subbands (2,0) and (2,1). This process is repeated to form the wavelet packet tree shown in Figure 4. The time series at the end of each "branch" are the final subbands used to represent the signal. For this simple tree, the original signal is broken up into the five subbands (1,1), (2,1), (3,0), (4,2), and (4,3).

After the signal is decomposed, the energy in each subband is calculated. Table 3 shows the approximate frequency range and the signal energy in each wavelet. The results of the energy analysis show that, besides the low frequency energy, the majority of the signal energy is contained in subband (4,2). The majority of the signal energy would be retained if subbands (3,0) and (4,2) are used to reconstruct the signal.

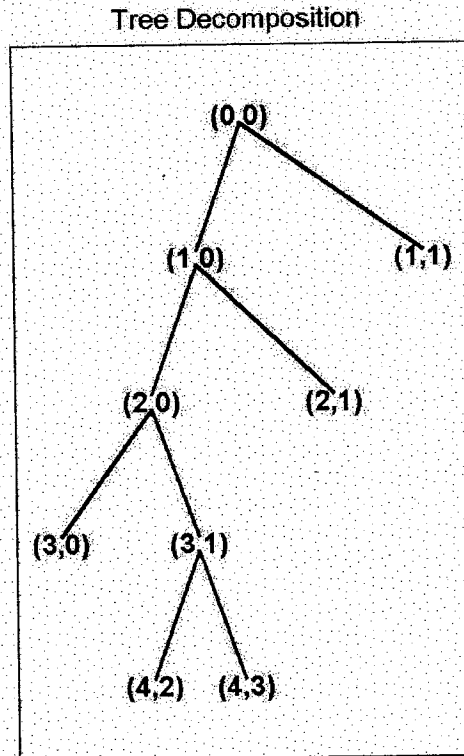


Figure 4. The wavelet packet tree used in wavelet filtering.

Subband	Approximate frequency range (Hz)	Subband Energy (% Total Energy)
(1,1)	15 - 30	0.003
(2,1)	7.5 - 15	0.014
(3,0)	0 - 3.75	95.25
(4,2)	3.75 - 5.625	4.53
(4,3)	5.625 - 7.5	0.22

Table 3 . Wavelet subband energy for synthetic anomaly signal.

### 3.2.2 Noise Signal

The noise signal was obtained from measured data taken at altitudes above 10 meters. At these altitudes, ground magnetic anomalies have a minimal influence on the magnetic measurements; the sensors respond primarily to the magnetic field of the helicopter and to fluctuations in the earth's magnetic field. The pure noise signal is shown in Figure 5. The approximate frequency range and the signal energy in each of the wavelet subbands

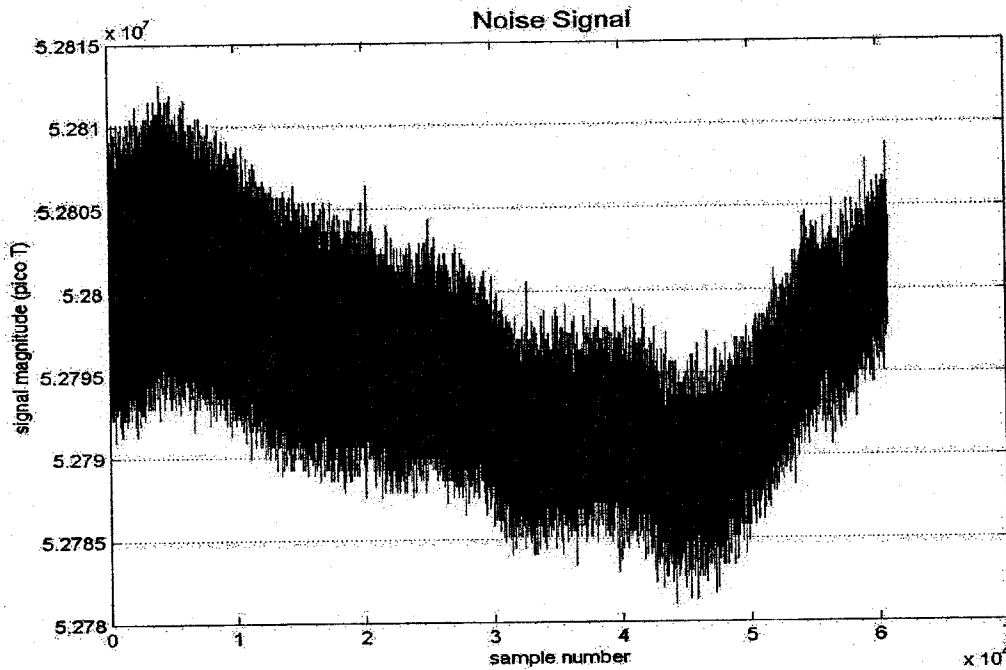


**Figure 5. The pure noise signal.**

are shown in Table 4. The results of the energy analysis show that, besides the low frequency energy, the majority of the signal energy is contained in subbands (1,1), (2,1), and (4,3). If these subbands are not included in the reconstructed signal, the majority of the noise at frequencies greater than 3.75 Hz would be eliminated. A standard regional correction or possibly high pass filtering could remove the low frequency noise.

Subband	Approximate frequency range (Hz)	Subband Energy (% Total Energy)
(1,1)	15 - 30	2.66
(2,1)	7.5 - 15	1.27
(3,0)	0 - 3.75	94.22
(4,2)	3.75 - 5.625	0.41
(4,3)	5.625 - 7.5	1.45

**Table 4 . Wavelet subband energy for measured noise signal.**

More can be said concerning neglecting the low frequency components to eliminate low frequency noise. Originally, we had tried using a longer wavelet decomposition that broke subband (3,0) and additional four levels. The lowest frequency subband contained a significant amount of noise energy and was neglected during signal reconstruction. The unexpected result was the appearance of a relatively large scale, low frequency artifact that distorted the data to the point of making it useless. For this reason, the low frequency subbands have been retained and this portion of the standard filtering (i.e., the regional correction) was used to remove the low frequency noise. It should be possible to develop a wavelet-based filtering scheme that will remove the low frequency noise without adding unacceptable artifacts; this investigation will be need to wait until the next phase of the follow-on project.

Additional insight into the performance of the wavelet decomposition can be obtained from the information shown in Figure 6. In this figure, the magnitudes of the discrete Fourier transform of each wavelet subband are shown. In addition to the obvious frequency range of each subband, the results in the frequency domain show the rotor noise at approximately 6.5 Hz and an unidentified frequency peak at 5 Hz. Based on the wavelet subband energy in the synthetic anomaly signal and the pure noise signal, the wavelet filtering scheme selected is to use only subbands (3,0) and (4,2) in the

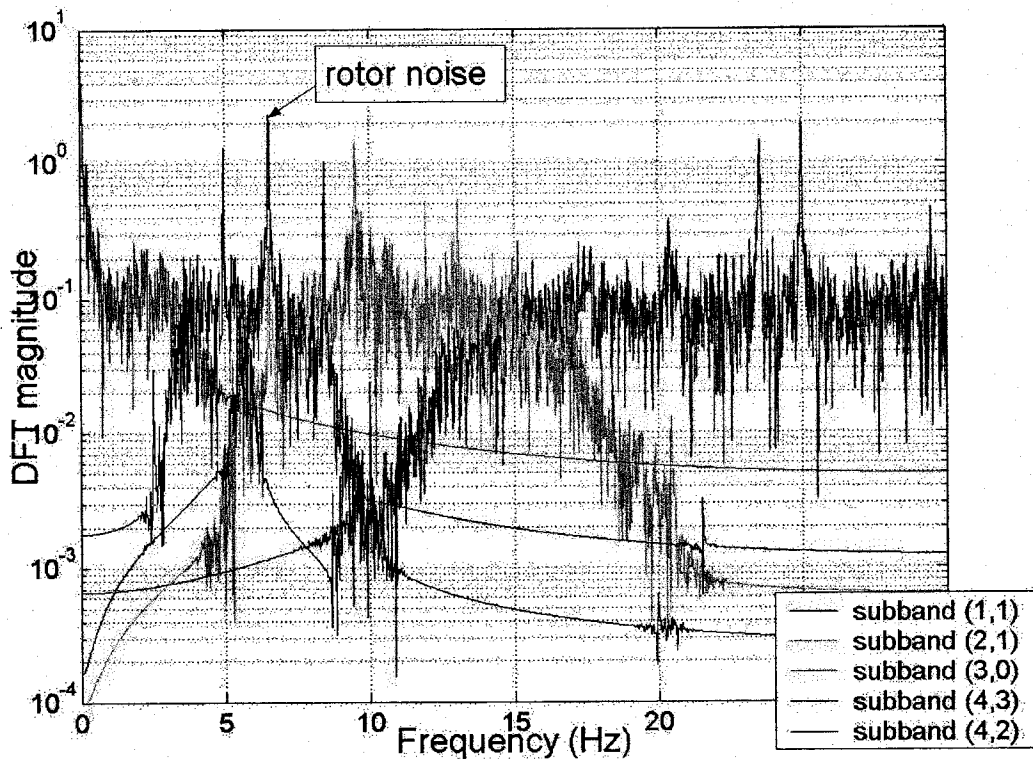


**Figure 6. Discrete Fourier transform magnitude of the wavelet subbands for the pure noise signal.**

signal reconstruction. Thus, the wavelet filtering will consist of decomposing the magnetometer signal by using the wavelet tree structure shown in Figure 4 (Daubechies 20 coefficient wavelet is used), and then reconstructing the filtered time series from subbands (3,0) and (4,2). This filtering scheme passes signals in the frequency range of 0 to 5.625 Hz, effectively eliminating the rotor noise.

### 3.3 Filtering Results

The wavelet filtering strategy was applied to data collected from the Badlands bombing range in September 2000. The data was collected by using the Oak Ridge Airborne Geophysical System – Hammerhead Array (ORAGS™-HA). Figure 7 shows the survey helicopter with the mounted ORAGS™-HA system.

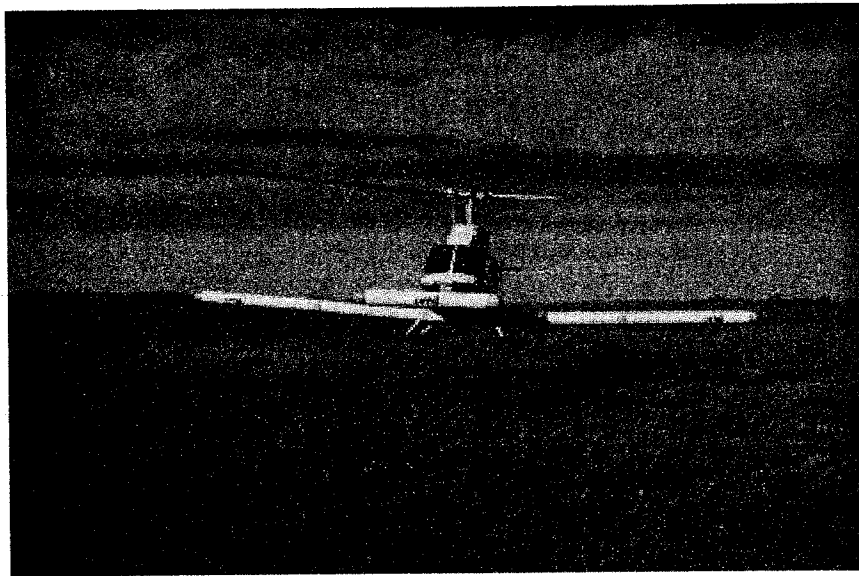
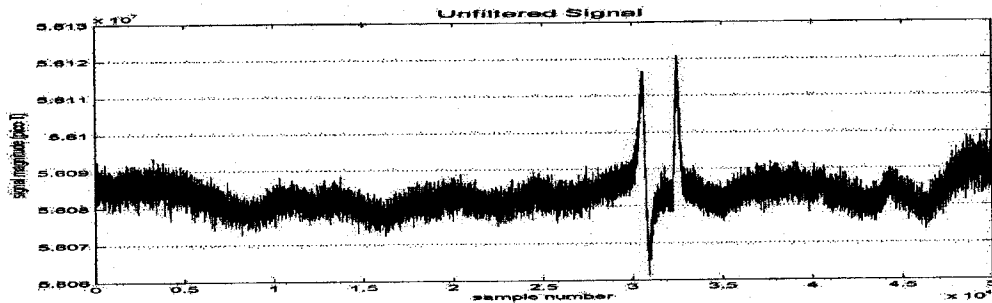


**Figure 7. The ORAGSTM Hammerhead array for UXO detection.**

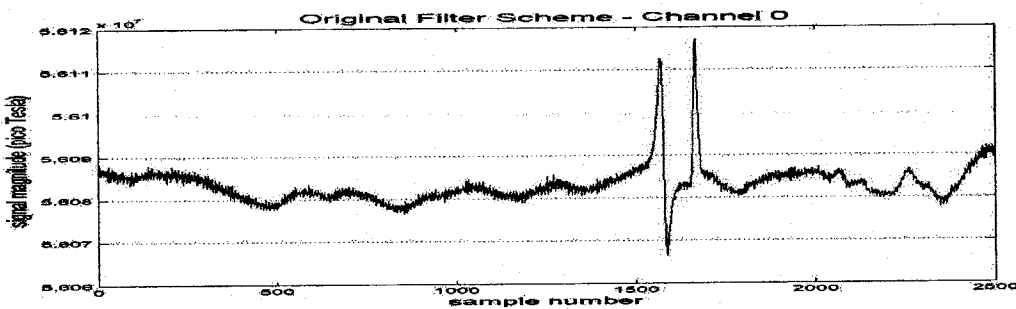
This system deploys 8 magnetometers at 1.75m with three magnetometers located in each of the lateral booms and two magnetometers located in the forward boom. The system uses a PC-based data acquisition system that is capable of recording raw synchronous Larmor frequency measurements from the magnetometers at 1200 Hz sample rate. The ORAGS system can record raw data at 1200 Hz sample rate; For these tests, data were downsampled to 60Hz in order to minimize the impact of power line interference.

Over 2200 acres of the BBR were surveyed with the ORAGS-HA system during a 10 day period in September 2000. This included a test site, five large target areas, and numerous transects. The test site and target areas were surveyed as part of an Environmental Science and Technology Certification Program (ESTCP) demonstration project, while the transects were surveyed to support ongoing Engineering Evaluation/Cost Analysis (EE/CA) efforts by Parsons Engineering Science. The test grid was 100m x 150m and included several pieces of ordnance that are not common at BBR, but frequently occur at

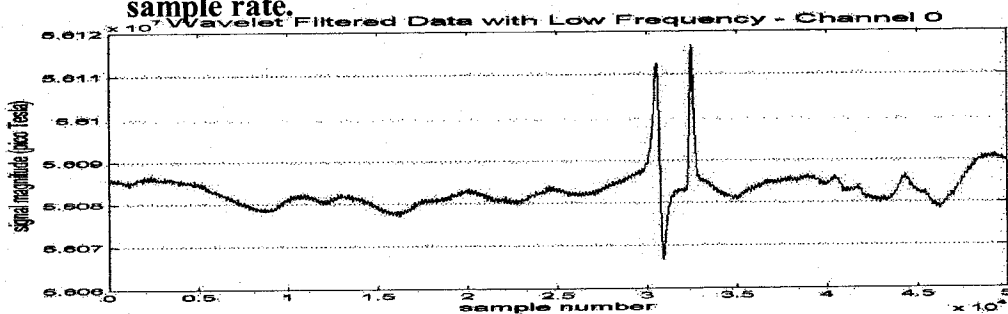
other UXO sites. These include 105mm and 155mm artillery, 20mm rounds, mortars and rockets. Figure 8 shows a portion of a typical magnetometer signal, in this case channel 0, as the helicopter passes over a magnetic anomaly. The presence of two magnetic anomalies is clearly shown, but also a considerable amount of noise (primarily rotor noise) can also be plainly seen. Three profiles are shown. The first shows the unfiltered data sampled at 1200 Hz. These data have undergone the compensation correction, but have had no additional signal processing. The second profile shows the data after standard filtering. In this case, the data was downsampled to 60 Hz before filtering. The results show a significant reduction in the noise level. The third profile shows the data after wavelet filtering. Here, the filtered data was upsampled to the original 1200 Hz sampling.



(a) - Unfiltered signal, sampled at 1200 Hz.



(b) - Results of current filter scheme signal, displayed at 60 Hz sample rate.



(c) - Wavelet-filtered signal, displayed at 1200 Hz sample rate.

Figure 8. Comparison of filter results on magnetic profile data.

A qualitative comparison of the filtered results shows that both accurately preserve the shape and amplitude of the peaks associated with the magnetic anomaly. However, the wavelet-filtered data has significantly less noise than the standard-filtered data. Thus, it appears that the wavelet filter is superior to the standard filter for removing noise.

Investigation of the filtered results in the frequency domain provides additional insight into the performance of the two filters. Figure 9 shows the filtered results in the frequency domain. The unfiltered signal shows the signal energy to be primarily at low frequencies with a prominent rotor noise peak at approximately 6.5 Hz and an unidentified noise peak at approximately 5 Hz. Some additional signal energy is present in the 13 to 15 Hz frequency range. After standard processing, the signal energy below approximately 4 Hz is preserved; the signal content above 4 Hz has been completely eliminated. The standard processing effectively removes the rotor noise, but also removes any information describing the magnetic anomalies between 4 and 6 Hz. The unidentified noise peak at 5 Hz is removed by the standard processing.

After wavelet-filtering, the signal energy is preserved up to a frequency of approximately 6 Hz. The rotor noise is effectively removed and additional information in the 4 to 6 Hz frequency range is retained. This additional information should result in a more detailed representation of magnetic anomalies in the wavelet-filtered data, compared to the standard-filtered data. The unidentified noise peak at 5 Hz is preserved in the wavelet-filtered data.

The filtered results can also be compared after gridding. The compensated data was filtered using both the standard filtering and wavelet-filtering. The two results were gridded by using GeoSoft software. The results are shown in Figures 10 and 11. Figure 10 shows a portion of the collected data for a relatively large area. Close examination of the figure shows the wavelet-filtered results to represent the magnetic anomalies with additional detail compared to the standard-filtered results. The region enclosed in the circle is expanded in Figure 11. Here, the additional detail preserved by the wavelet filtering is clearly evident. Not only are more anomalies shown, but the anomalies shown when using standard filtering are shown with additional detail when wavelet filtering is used. This additional detail can be attributed to the additional information in the 4 to 6 Hz frequency range that is preserved by wavelet filtering.

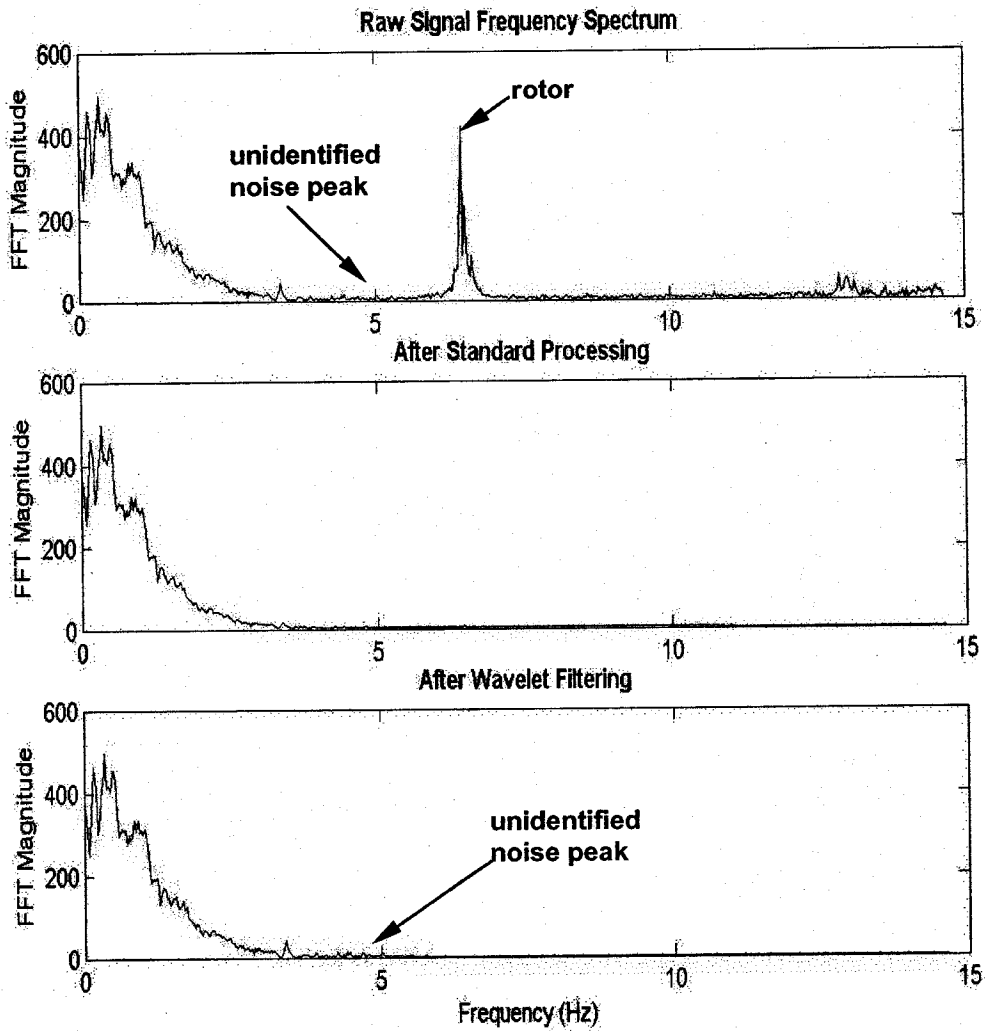


**Figure 9. Comparison of filtered profile data in the frequency domain.**

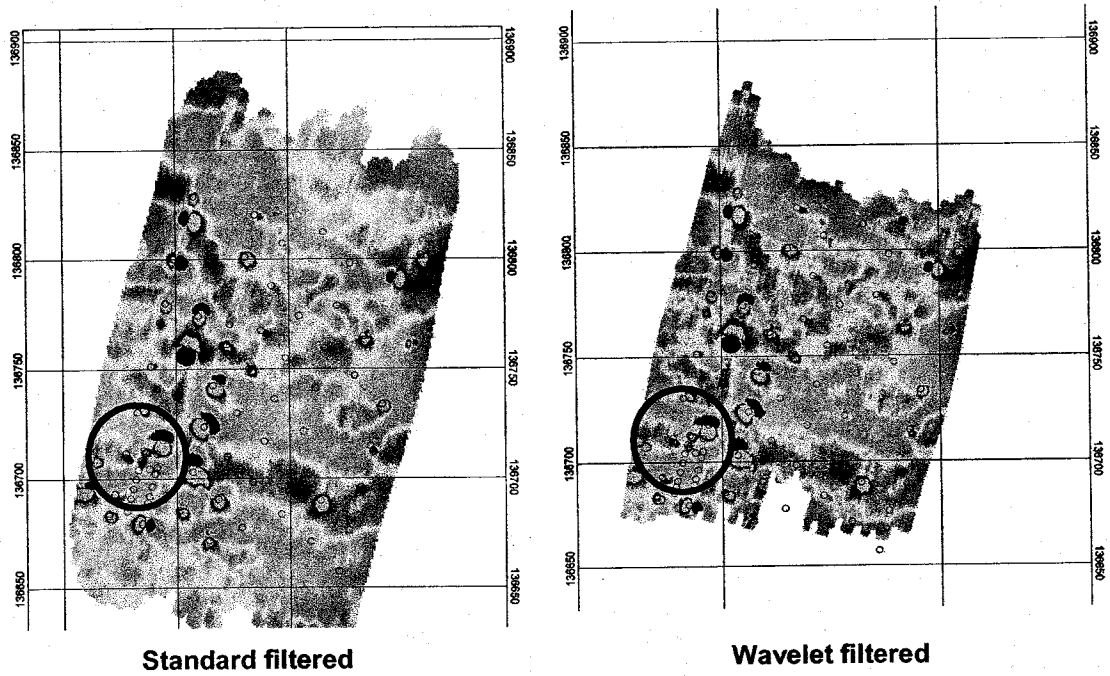


**Figure 10. Comparison of standard-filtered and wavelet filtered gridded data - large area view.**

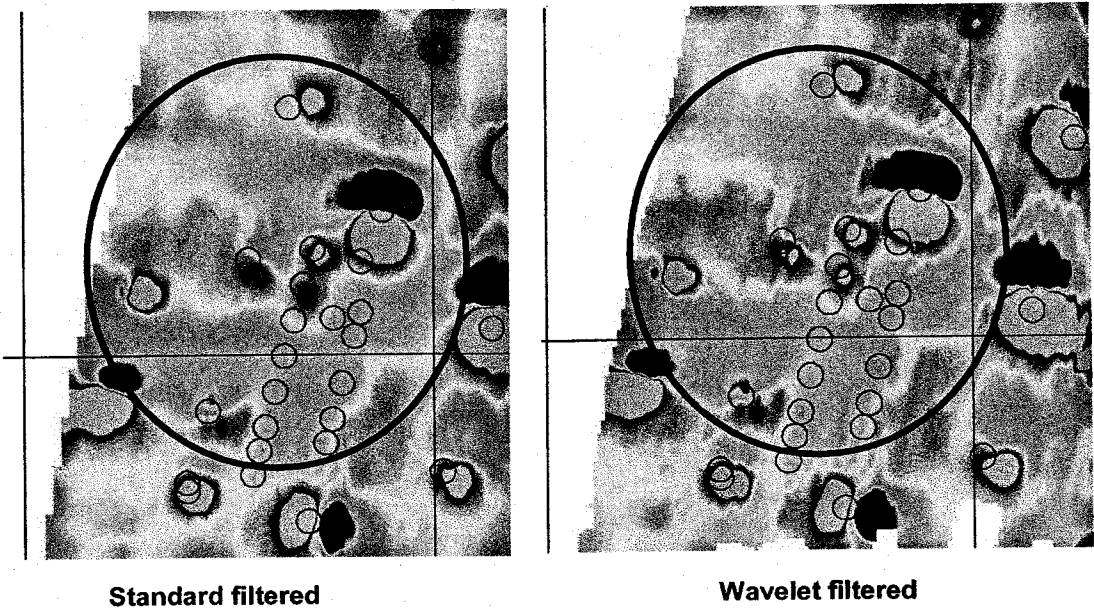


**Figure 11. Comparison of standard-filtered and wavelet filtered gridded data - detailed view.**

A quantitative measure of the difference between standard filtering and wavelet filtering can be obtained from analysis of high-altitude noise data. The measured signal, which is collected at altitudes greater than ten meters, can be filtered using each filtering method and the filtered results quantitatively compared. Figure 12 shows the frequency domain representation between 0 and 7 Hz of a sample of high altitude data after filtering using both methods. The results show that both filtering methods are practically identical at frequencies below 4 Hz. Between 4 and 6 Hz, the wavelet filtering preserves more of the signal, a result previously shown in Figure 9. Between 6 and 7 Hz, the frequency band containing rotor noise, it is seen that the wavelet filtering removes more of the signal. Figure 13 shows the comparison of the two filtering method results in more detail over the frequency range of 4 to 7 Hz.

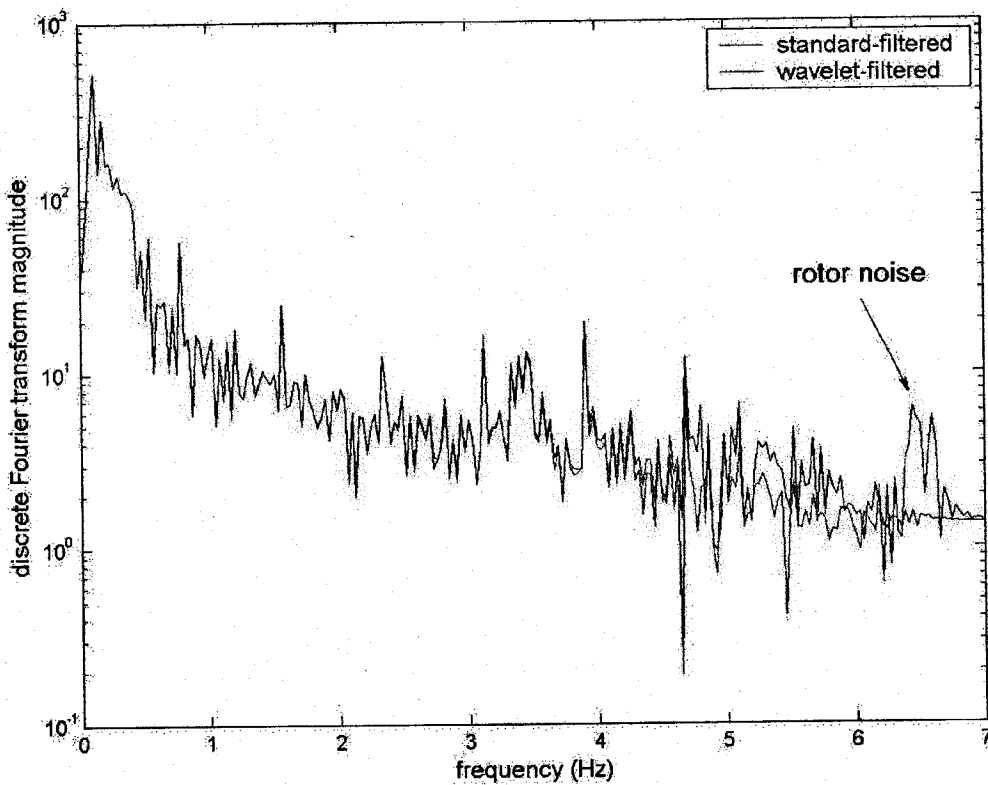


**Figure 12. Frequency domain comparison of high altitude noise filtered using standard and wavelet filtering – 0 to 7 Hz.**

A measure of the relative energy in each filtered signal can be made by integrating the filtered results over frequency. The ratio of the energies in each signal indicates the relative magnitude of the energy content of the filtered signals. Table 5 shows the ratio of the signal energy of the two filtering methods over the frequency ranges of 0 to 4 Hz, 4 to 6 Hz, and 6 to 7 Hz. The results show that the two filtering methods have nearly identical energies over the frequency range of 0 to 4 Hz. Wavelet filtering retains approximately 42% more signal energy over the frequency range of 4 to 6 Hz. Over the

frequency range of 6 to 7Hz, wavelet filtering removes 34% more noise than standard filtering. Thus, for this case (which we believe to be representative of noise in the ORAGS™-HA system), wavelet filtering retains 42% more energy in the 4 to 6 Hz frequency range while rejecting 34% more noise in the 6 to 7 Hz frequency range.

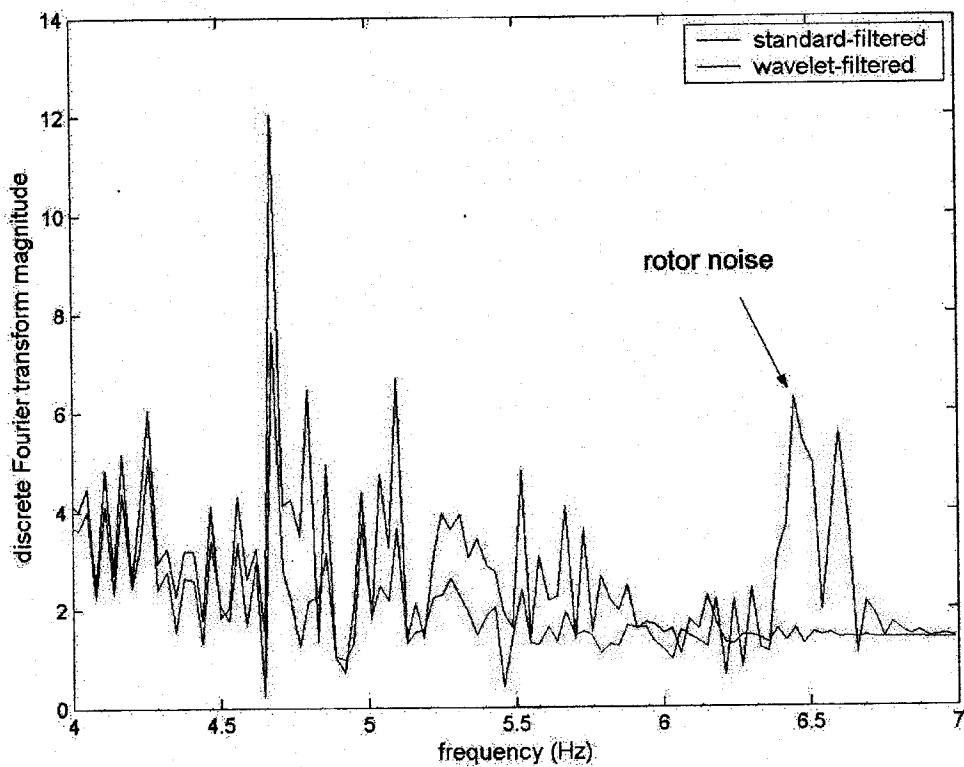


Figure 13. Frequency domain comparison of high altitude noise filtered using standard and wavelet filtering – 4 to 7 Hz.

Frequency Range (Hz)	Signal Energy Ratio (wavelet energy/standard energy)	% Additional Energy in Wavelet-Filtered Signal
0 - 4	1.004	0.42%
4 - 6	1.425	42.5%
6 - 7	0.66	-34%

Table 5. Comparison of energy content of the filtered signals.

A comparison of the ease of application can be made between the two filtering methods. Figure 14 compares block diagrams of the filtering steps for the standard filtering, the current wavelet filtering, and our expectation of the future wavelet-filtering processes. Currently, standard filtering requires more steps than the wavelet filtering. Furthermore, some of the filtering steps, such as comparing regional corrections and making the B-Spline fit, require user intervention or input. This intervention may be relatively benign when filtering small data sets, but can significantly increase the time and cost for filtering large data sets and such intervention requires a highly skilled analyst.

Wavelet filtering greatly simplifies filtering by eliminating several of the current processing steps, including some that require user intervention or input. Future wavelet filtering, which would involve converting the wavelet filtering into a GeoSoft module,

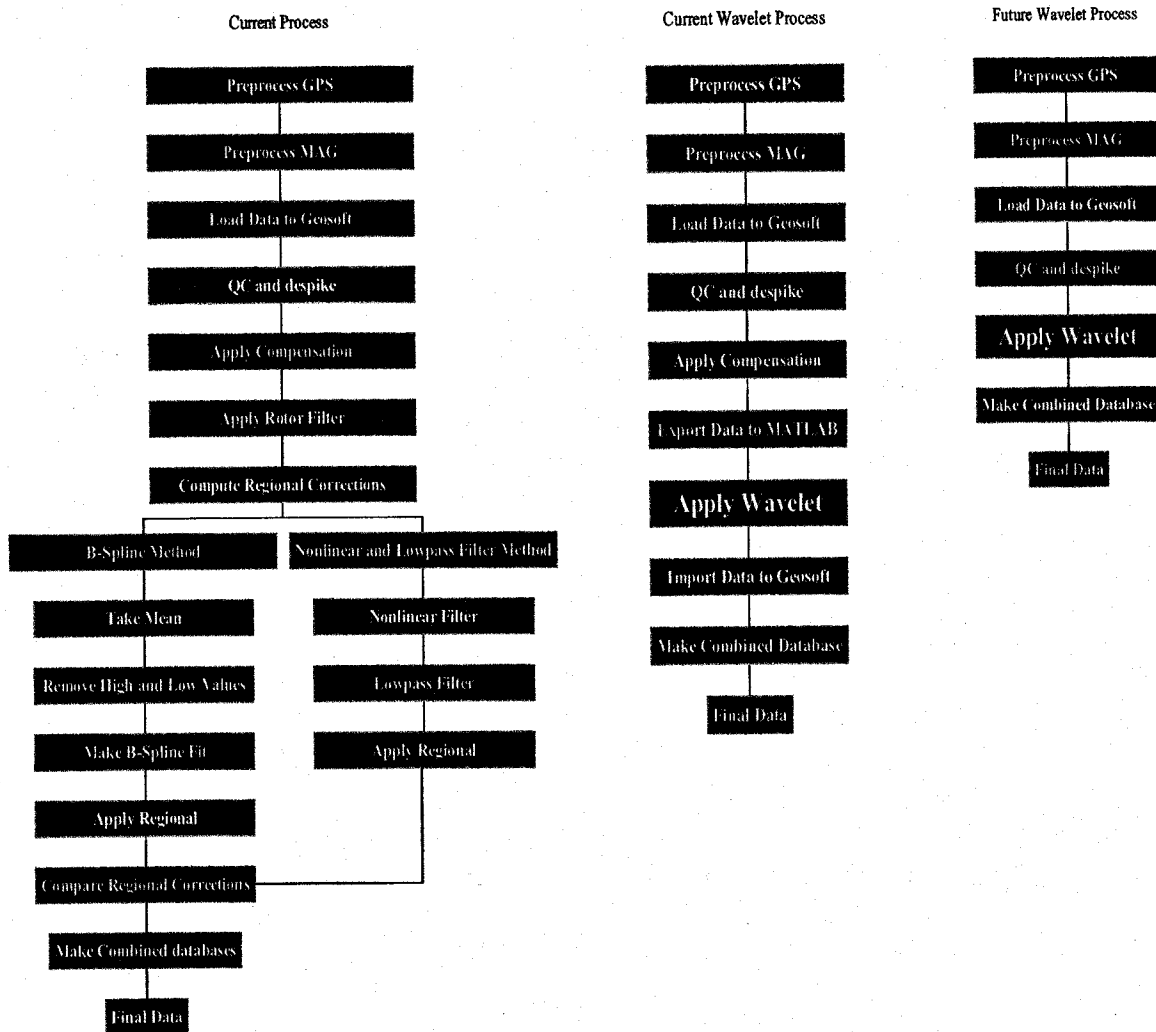


**Figure 14. Block diagram comparing the filtering steps for standard filtering, wavelet filtering, and the expected final wavelet filtering processes.**

would simplify filtering even further, possibly making it essentially a "turn-key" operation that can be performed without user interaction. It is expected that the application of wavelet filtering can significantly decrease the manpower, time, and ultimately the cost required to filter large data sets. Such data sets will become common as airborne data acquisition is used to survey more UXO sites.

### **3.4 - Summary of Wavelet Filtering Results**

The results of comparing standard filtering with wavelet filtering indicate the following:

- 1) Wavelet filtering removes more noise at frequencies above 6 Hz than standard filtering. This result is qualitatively shown in Figures 8, 12, and 13. For the analyzed noise sample it was found that wavelet filtering removed approximately 34% more noise in the 6 to 7 Hz frequency range than did standard filtering.
- 2) Wavelet filtering preserves more useful information in the 4 to 6 Hz frequency range than standard filtering. This result is shown in the comparison of the frequency content of the two filtering methods shown in Figures 9, 12, and 13 and in the comparison of the gridded data shown in Figures 10 and 11. For the analyzed noise signal it was found that wavelet filtering preserved approximately 42% more signal in the 4 to 6Hz frequency range than did standard filtering.
- 3) Wavelet filtering is simpler and requires less user intervention than current filtering. It is expected that wavelet filtering can be further simplified by incorporating the filtering into a GeoSoft module.

## **4 - DISCRIMINATION OF ORDNANCE AND CLUTTER**

As described above, we were limited in this project to identifying a partial descriptor set for use in determining if a magnetic anomaly represents ordnance or clutter. This descriptor set identification was done with an extremely limited number of measured samples of ordnance and clutter. The samples used in this evaluation were two practice bombs, a barbed wire fragment, a bomb fin, and magnetically responsive soil. Two channels of measured data were used in the evaluation of each sample.

### **4.1 Descriptor Selection and Evaluation**

Our efforts focused on evaluating the potential of three algorithmically-derived descriptors; wavelet subband energy, signal entropy, and the discrete Fourier transform spectra. Wavelet subband energy measures the amount of signal energy in a particular wavelet subband. This quantity indicates the frequency distribution of energy in a signal. It is reasonable to expect that the energy distribution of relatively large, intact metallic bodies such as ordnance will have different energy distributions than smaller, distributed metallic bodies. Signal entropy is a measure of correlation or noise in a signal. Again, it is expected that ordnance signals would have relatively highly correlated signals,

resulting in relatively low entropy. Clutter signals should be less correlated, resulting in relatively high entropy. The discrete Fourier transform is another measure of the distribution of signal energy over frequency. A comparison of the descriptor values for each of the samples is presented in this section.

#### 4.1.1 Wavelet Subband Energy

A four level dyadic wavelet decomposition was used on the sample signals. An 8-coefficient Daubechies wavelet was used in the decomposition. The wavelet tree structure describing the decomposition is shown in Figure 15. The energy of subband (4,1) was used as the descriptor. This subband corresponds to an approximate frequency range of 1.5 to 4 Hz. Figure 16 shows the subband energy as a percentage of the total energy in the signal. The sample number corresponds to the two data channels for the two practice bombs and the two data channels for the bomb fin, barbed wire sample, and magnetically responsive soil. The results show that in general the practice bombs have a much higher percentage of signal energy in subband (4,1) than the bomb fin, barbed wire sample, or the magnetically responsive soil. The one exception is one barbed wire sample that contains an energy equivalent to the practice bomb.

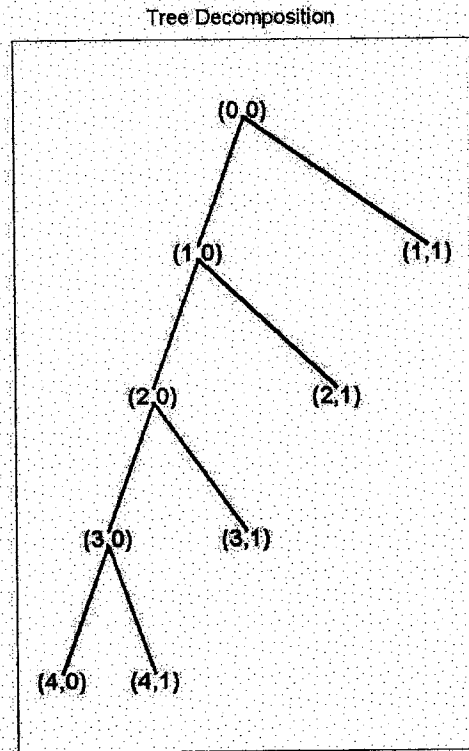


**Figure 15. Four-level dyadic wavelet tree structure used in the wavelet decomposition**

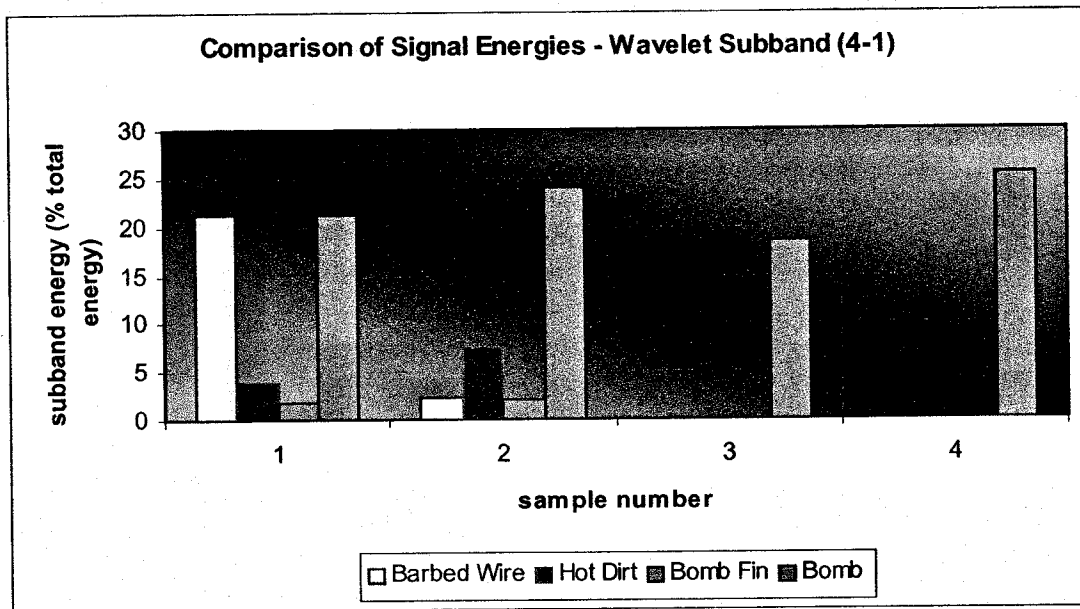


Figure 16. Signal energies for wavelet subband (4,1).

#### 4.1.2 Signal Entropy

The signal entropy for the descriptor samples is shown in Figure 17. As expected the entropy for the practice bombs are considerably less than that of the clutter objects. Again, the one exception is one of the barbed wire samples, which has a similar entropy value to the practice bombs.

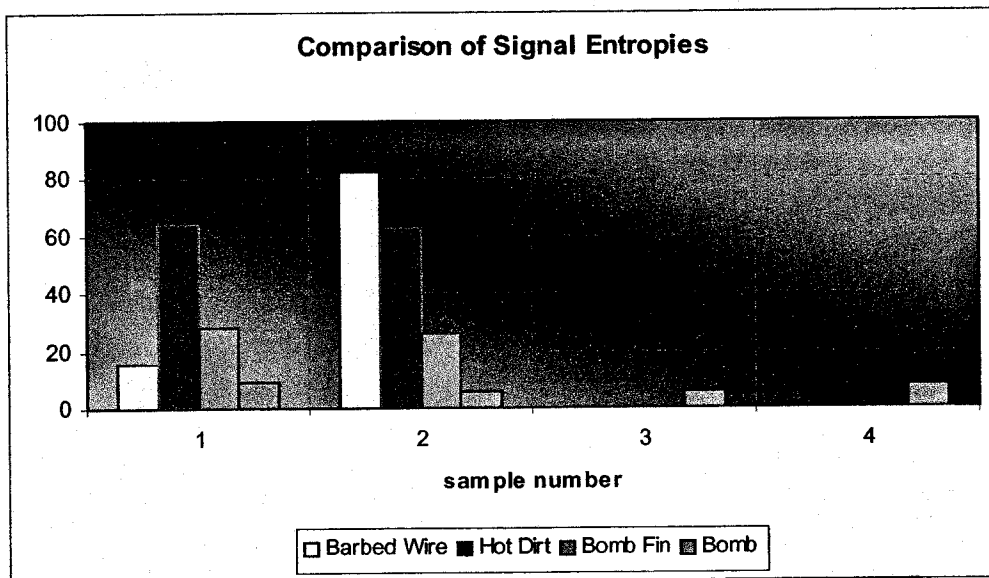


Figure 17. Signal entropies.

### 4.1.3 Discrete Fourier Transform

The discrete Fourier transform is another measure of the energy distribution of a signal. Figure 18 shows the Fourier spectra of the descriptor samples. To generate the spectra shown in this figure, each of the sample signals was first normalized to have a peak response magnitude of  $\pm 1.0$ . Comparing the results, one sees that the spectra of the ordnance and clutter examples are quite different. In general, the spectra of the ordnance are relatively flat with no prominent peaks in the 0 to 4 Hz frequency range. The spectra of the clutter samples show significant peaks in the 0 to 4 Hz frequency range and contain less energy (as a percentage of total energy) in the 2 to 4 Hz frequency range. Although not done in this investigation, it should be possible to select additional descriptors from the discrete Fourier transform to distinguish between ordnance and clutter.

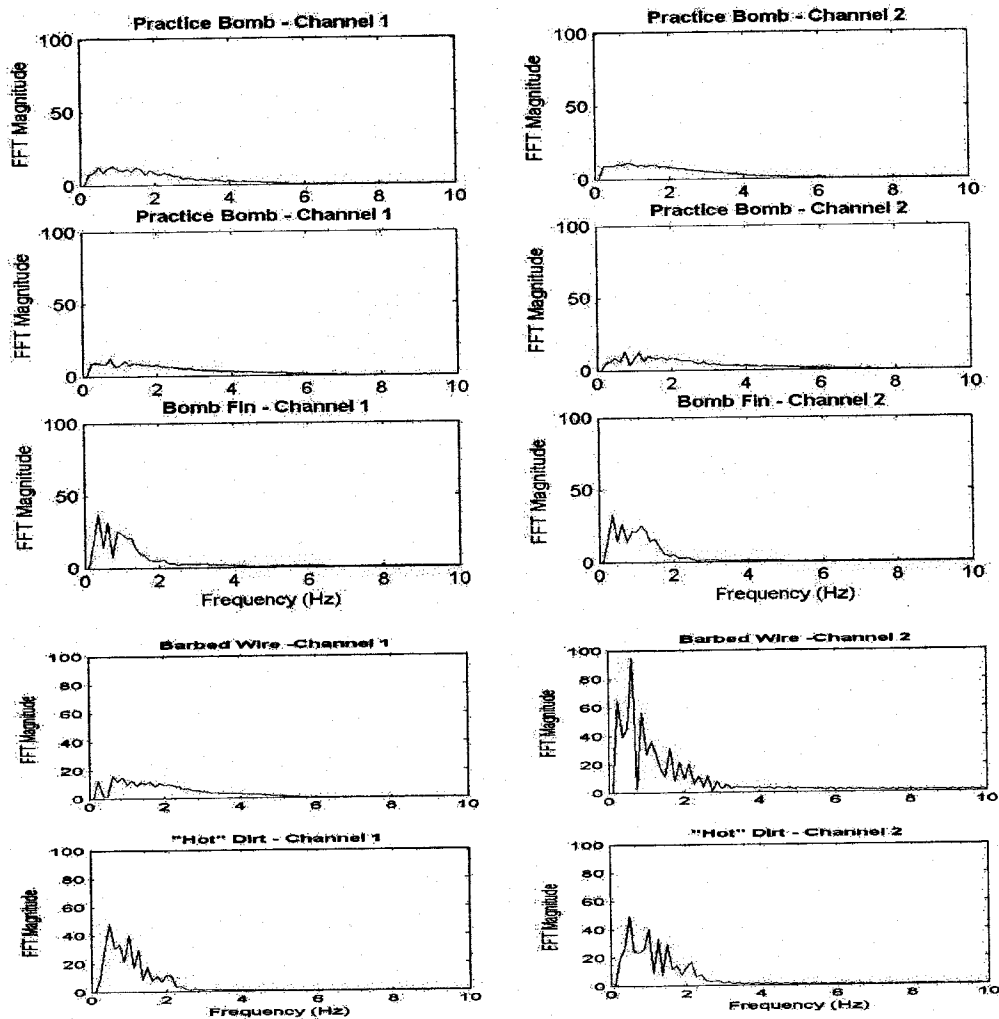


Figure 18. Discrete Fourier transforms spectra.

## 5 –CONCLUSIONS AND RECOMMENDATIONS

Based on our results, we believe the following conclusions are justified:

1) Wavelet filtering removes more noise at frequencies above 6 Hz than standard filtering. This result is qualitatively shown in Figures 8, 12, and 13. For the analyzed noise sample it was found that wavelet filtering removed approximately 34% more noise in the 6 to 7 Hz frequency range than did standard filtering.

2) Wavelet filtering preserves more useful information in the 4 to 6 Hz frequency range than standard filtering. This result is shown in the comparison of the frequency content of the two filtering methods shown in Figures 9, 12, and 13 and in the comparison of the gridded data shown in Figures 10 and 11. For the analyzed noise signal it was found that wavelet filtering preserved approximately 42% more signal in the 4 to 6Hz frequency range than did standard filtering.

3) Wavelet filtering is simpler and requires less user intervention than current filtering. Figure 12 compares the application of the two methods. It is expected that wavelet filtering can be further simplified by incorporating the filtering into a GeoSoft module. This reduction in complexity would result in significant savings in both time and cost, especially if large areas are to be surveyed.

4) The very preliminary work done during this study encourages us that a descriptor set that can be used to distinguish between ordnance and clutter can be identified. This descriptor set would most likely include the descriptors used in this study but would probably include additional descriptors. If such a descriptor set can be identified, it should be possible to use these descriptors with probabilistic methods to classify a magnetic anomaly as being either ordnance or clutter.

We recognize that the number of ordnance and clutter samples prevents a statistically valid determination on the ability of the descriptor set to distinguish between ordnance and clutter. However, because the limited results are so unambiguous, we feel confident in concluding that there is real potential for identifying a descriptor set that will accurately distinguish between ordnance and clutter.

Based on our results, we believe that both wavelet filtering and the application of probabilistic methods for distinguishing ordnance from clutter have potential for improving the detection and identification of UXO. We recommend that a follow-on project be initiated to

1) Fully develop the wavelet filtering technique and incorporate the final wavelet filtering into a GeoSoft module. This module would be made available to the UXO community and should result in the extraction of more useful information from the measured data than is currently being obtained. In addition to the improvement in filtering performance,

we believe that the use of wavelet filtering will reduce the time, manpower, and cost of filtering the large data sets typically collected by airborne UXO surveys.

2) Fully explore the potential of wavelet-based descriptors and probabilistic methods for discriminating between ordnance and clutter. The preliminary work shown here appears promising but is only a start in evaluating the potential of this approach. Evaluation using larger data sets involving many more examples of ordnance and clutter objects is needed to determine if an effective descriptor set can be identified. If successful, this approach would form the basis for a screening of magnetic anomalies, allowing analysts to focus on only the most promising anomalies. Again, a reduction in the time, manpower, and cost of evaluating the survey results would be achieved.

## REFERENCES

1. Akansu, A. N., and R. A. Haddad, *Multiresolution Signal Decomposition*, 1992, Academic Press, Inc., San Diego, CA., pp. 292-313.
2. Daubechies, I., *Ten Lectures on Wavelets*, 1992, Society for Industrial and Applied Mathematics, Philadelphia, pp. 199-209.